Available online at https://sej.journals.ekb.eg/

FACULTY OF ENGINEERING – SOHAG UNIVERSITY

SOHAG ENGINEERING JOURNAL (SEJ), VOL. 1, NO. 1, MARCH 2021

SENSORLESS VECTOR CONTROLLED THREE-PHASE PWM INVERTER-FED INDUCTION MOTOR DRIVE SYSTEM WITH AUTO-TUNING ESTIMATION OF MACHINE PARAMETER APPROACH

Khairy Sayed* and Ahmed M. Kassem

Electrical Engineering Department, Sohag University, 82524, Sohag, Egypt

Abstract

This paper deal with a practical development technology on a highly accurate faster response adjustable speed drive implementation for the three-phase sinewave fed general purpose induction motor system which is based upon sensorless slip frequency type vector control scheme with an automatic auto-tuning machine parameter estimation strategy. The essential procedure and considerations to measure and estimate the exact stator and cage rotor circuit parameters of the induction motor treated here are discussed under its operating conditions. The speed regulation characteristics of the induction motor is illustrated and evaluated for the induction machine parameter variations under the actual operating conditions ranging from a low frequency to a high frequency for various specified load torque setting. The variable speed induction motor drive system employing sensorless slip frequency-based vector control scheme which incorporates the current controlled three-phase high frequency carrier PWM switching inverter with automatic auto-tuning estimation strategy on the temperature-dependent and -independent machine circuit parameters is practically implemented using DSP-based vector controller. The dynamic speed response performances under essentially changed load torque disturbances as well as steady state speed against torque characteristics of the proposed variable speed drive control and implementations are illustrated and discussed from an experimental point of view.
 DOI: 10.21608/SEJ.2021.155853.

Keywords: Induction Motor Variable Speed Drive, Sensorless Slip Frequency-based Vector Control, Three-phase Sinewave PWM Inverter, Auto-Tuned Machine Parameters Estimation, High accurate quick response.

1. INTRODUCTION

In recent years, a variety of latest power electronic associated control systems integration technologies relating to the high performance and wide range adjustable-speed drives for the general-purpose induction motor applications which are basically based on the three-phase voltage-source current-controlled PWM inverter using IGBTs and its associated slip frequency type vector control scheme have gained specific interest in the fields of the industrial, transportation, medical imaging equipment and consumer AC motor variable speed drives as well as electric vehicle AC motor variable speed drives. Thus, the exact stator and rotor circuit parameters of multi diverse general-purpose induction different types of motors driven under specified various load working conditions should be measured in real time processing and estimated automatically in the case of a temperature dependent parameters variation for the purpose of sensorless slip frequency-based vector control implementation introduced for the induction motor variable-speed drive systems. In particular, the complex temperature-

* Corresponding author. khairy_sayed@eng.sohag.edu.eg

dependent rotor resistance variations of application specific induction motors and different rated induction motors are considered and influence upon not only the steady state speed regulation in accuracy but also for the settling time at the transient speed responses. It is difficult to achieve the sufficient speed regulation precision on in steady state as well as the speed settling time in dynamic operating state which are practically required for wide speed setting ranges and largely changed load torque disturbances for the general-purpose induction motors. In order to solve these feasible problems significant mentioned above, the authors have recently developed a simple and practical automatic autotuning method to measure and estimate the exact stator winding and cage type rotor circuit parameters of application specific type induction motors in addition to some different type of general-purpose induction motors used widely from multi-diverse utilization viewpoints.

In addition to these, the high precision performance induction motor variable speed electrical drive system operated by the sensorless vector control based three-phase voltage source PWM inverter with a specific automatic autotuning machine parameter estimation processing approach is newly introduced for compensating the transient torque current component due to transient current suppression from a practical point of view.

This paper presents the state-of-the art feasible development and characterization on the general purpose and application specific induction motor variable speed drive system applied for multi-diverse industrial fields which are based upon the sensorless slip-frequency vector control implementation with a novel automatic autotuning type machine parameter estimation strategy. The experimental results obtained from the slip frequency-based vector control induction motor adjustable drive system treated here are illustrated and discussed for speed regulation characteristics in steady state in addition to speed settling performances in dynamic state. The effectiveness of this variable speed system is proved and discussed from a practical point of view.

2. SYSTEM DESCRIPTION AND VECTOR CONTROL STRATEGY

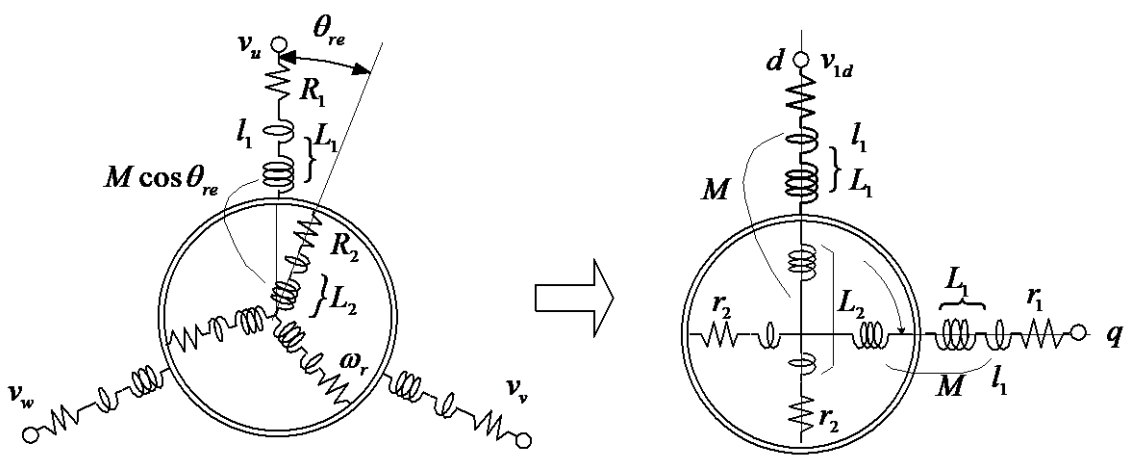

Fig. 1. Equivalent dynamic circuit of induction motor on plane transformed to d-q coordinate frame axis r_1: Stator resistance, r_2: Rotor resistance, L_1: Stator inductance, L_2: Rotor resistance, l_1: Stator leakage Inductance, l_2: Rotor leakage inductance, v_{1d}: Input voltage of d-axis, v_{1q}: Input voltage of q-axis, ω_s: Slip angular frequency, M: Mutual inductance between $L_1$and L_2.

An electrical dynamic equivalent circuit of the three-phase induction motor with cage rotor shown in Fig.1 which is represented on the d-q coordinate axis. Fig. 2 shows an adjustable-speed induction motor drive system by slip frequency mode vector control formulation based on the three-phase voltage source PWM inverter using the latest IGBT power modules. The induction motor variable speed drive system treated here incorporates the PI controller which has a delay function of the torque current component in order to suppress the transient current sufficiently under largely changed load conditions. In Fig.2, the flux linkage ϕ defined here equals to $L_1 i_{1d}$, in which L_1 is the stator inductance and i_{1d} is the d-axis exciting current component. Equation (1) gives the general voltage equation of induction motor described and formulated on rectangular coordinate of d-q frame coordinate, in which the rotation angular frequency denoted as ω.

$$\begin{bmatrix} v_{1d} \\ v_{1q} \\ 0 \\ 0 \end{bmatrix} = \begin{bmatrix} r_1 + \sigma L_1 p & -\sigma L_1 \omega & (M/L_2)p & -(M/L_2)\omega \\ \sigma L_1 \omega & r_1 + \sigma L_1 p & (M/L_2)\omega & (M/L_2)p \\ -Mr_2/L_2 & 0 & r_2/L_2 + p & -\omega_s \\ 0 & -Mr_2/L_2 & \omega_s & r_2/L_2 + p \end{bmatrix} \begin{bmatrix} i_{1d} \\ i_{1q} \\ \varphi_{2d} \\ \varphi_{2q} \end{bmatrix} \quad (1)$$

where i_{1d} is the d-axis exciting current component, i_{1q} is the q-axis torque current component, L_1 is the stator inductance, L_2 is the rotor inductance, r_1 is the stator resistance, r_2 is the rotor resistance,p is the differential operator ($= d/dt$), ω is the angular velocity value calculated in vector controlled sesorless inverter system, σ is the magnetic coupling coefficient of leakage flux, M is the mutual inductance between $L_1$and L_2, v_{1d} is the input voltage of d-axis, v_{1d}^* is the initial value of d-axis, v_{1q} is the input voltage of q-axis, and ϕ_{2d}, ϕ_{2q} are the d axis and q axis components of the rotor flux linkage described by

$$\phi_{2d} = Mi_{1d} + L_2 i_{2d} \quad \phi_{2q} = Mi_{1q} + L_2 i_{2q} \quad (2)$$

Equation (3) is a state-space vector equation estimated by rewriting (1).

$$p\begin{bmatrix} \sigma L_1 i_{1d} \\ \sigma L_1 i_q \\ \varphi_{2d} \\ \varphi_{2q} \end{bmatrix} = \begin{bmatrix} -r_1 - (M/L_2)^2 r_2 & \sigma L_1 \omega & (Mr_2/L_2)^2 & (M/L_2)\omega_r \\ \sigma L_1 \omega & -r_1 - (M/L_2)^2 r_2 & -(M/L_2)\omega_r & (M/L_2)^2 \\ Mr_2/L_2 & 0 & -r_2/L_2 & \omega_s \\ 0 & Mr_2/L_2 & -\omega_s & r_2/L_2 \end{bmatrix} \begin{bmatrix} i_{1d} \\ i_{1q} \\ \varphi_{2d} \\ \varphi_{2q} \end{bmatrix} + \begin{bmatrix} v_{1d} \\ v_{1q} \\ v_{2d} = 0 \\ v_{2q} = 0 \end{bmatrix} \quad (3)$$

where ω is the angular velocity value calculated in vector controlled sesorless inverter system, ω_s is the slip angular frequency, and ω_r is the rotor shaft angular frequency.

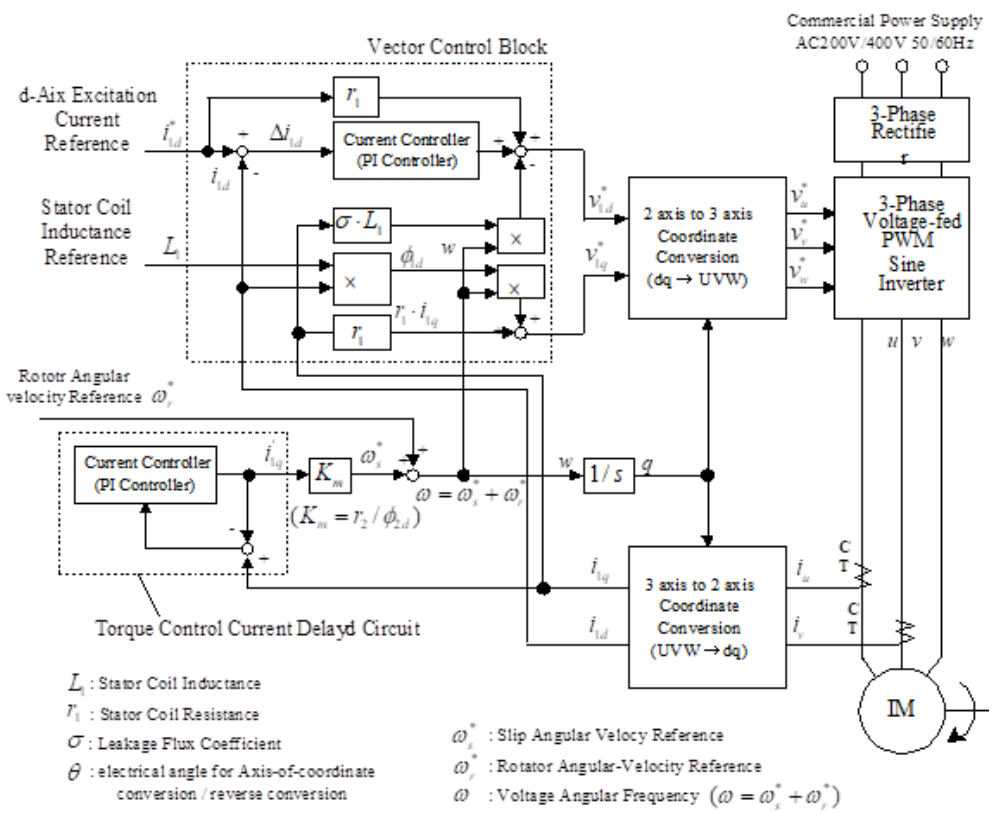

Fig. 2. Schematic block diagram of sensorless vector-controlled inverter system for induction motor variable speed drive.

The reference value ω_s of slip angular frequency can be mathematically formulated by the equation (4) considering L_2 and r_2, because the stator voltage and the stator current of the three phase cage rotor type induction motor operated on the basis of slip frequency type sensorless vector control principle are to be controlled as to be $\phi_{2d} = Mi_{1d}$ which is kept constant and $\phi_{2q} = 0$ regarding equation (3).

$$\omega_s = \frac{r_2 M}{L_2 \varphi_{2d}} i_{1q} \cong \frac{r_2}{\varphi_{2d}} = K_m i_{1q} \tag{4}$$

where $K_m = r_2/\phi_{2d}$.The angular slip frequency L_2 and r_2-based vector controlled three-phase PWM inverter provides the specific voltage vector equation expressed by the equation (5) derived from the equations (3) and (4).

Substituting $\phi_{2d} = Mi_{1d}$ which is kept constant and $\phi_{2q} = 0$ to the equation (1) for the three-phase induction motor under a steady state condition.

$$\begin{bmatrix} v_{1d} \\ v_{1q} \end{bmatrix} = \begin{bmatrix} r_1 & -\sigma L_{1d} \\ L_1 \omega & r_1 \end{bmatrix} \begin{bmatrix} i_{1d} \\ i_{1q} \end{bmatrix} \tag{5}$$

Under steady state condition, ω_s is calculated from the torque current component i_{1q} by the equation (4) and the rigid rotor shaft mechanical angular velocity ω_r of the induction motor could be coincided with the reference value of the stator angular frequency specified by adding ω_s^* to rotor angular speed reference ω_r^*.

In a transient condition, the slip angular frequency ω_s is formulated by equation (6) on the basis of substituting equation (5) to equation (3). As a result, ω_s can be obtained by the following equation:

$$\omega_s = \frac{r_2 M}{L_2 \varphi_{2d}} i_{1q} + \frac{\sigma L_1 M}{L_2 \varphi_{2d}} p i_{1q} \tag{6}$$

Based on equation (6), not only proportional term of torque current component i_{1q} but also differential term of i_{1q} determine the slip frequency angular ω_s.

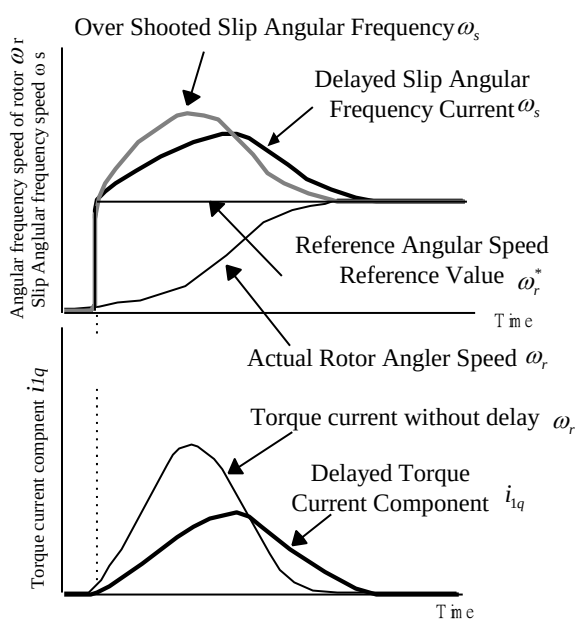

Fig. 3. Influence in case of transient mode of in the case of increasing torque current component.

Then calculated reference value of the stator angular frequency ω_s^* can be larger by the differential term specified by the equation (6). Therefore, it will be difficult to realize stable speed-adjustment in accordance with increasing of the slip angular frequency. The motor shaft mechanical angular speed value of ω_r can be regulated without making largely drastic changes of the reference slip frequency value of ω_s^*. The reference slip angular frequency ω_s^* is calculated by substituting the output value of the PI controller in which its input signal is the detected torque current component i_{1q}, as indicated in equation (4) mentioned above.

3. NOVEL PRACTICAL APPROACH OF MACHINE PARAMETER DETERMINATION

In this section, the novel automatic autotuning scheme of the three-phase induction motor machine parameters (L_1,L_2,r_1,r_2) is described that is necessary to be driven by slip frequency-based three-phase PWM vector-controlled inverter.

3.1. Influence on the errors of motor parameters (L_1,L_2,r_1,r_2) value preset to the inverter.

The three-phase voltage-fed type inverter supplies the voltage compensated for the voltage drop by the rotor resistance r_1 and the stator resistance r_2 of the test motor itself to provide the required current to the induction motor. Therefore, it is noted that the error between the measured value and the actual value of the induction motor parameters, the stator resistance r_1 and the stator inductance L_1 become the error of the motor current value.

On the other hand, the equivalent resistance r_2 of the rotor of the induction motor is to be contained in the proportional coefficient for dynamic slip angular frequency from a torque current component in Equation (6), the measurement error of a rotor resistance r_2 is to cause an error of slip angular frequency ω_s.

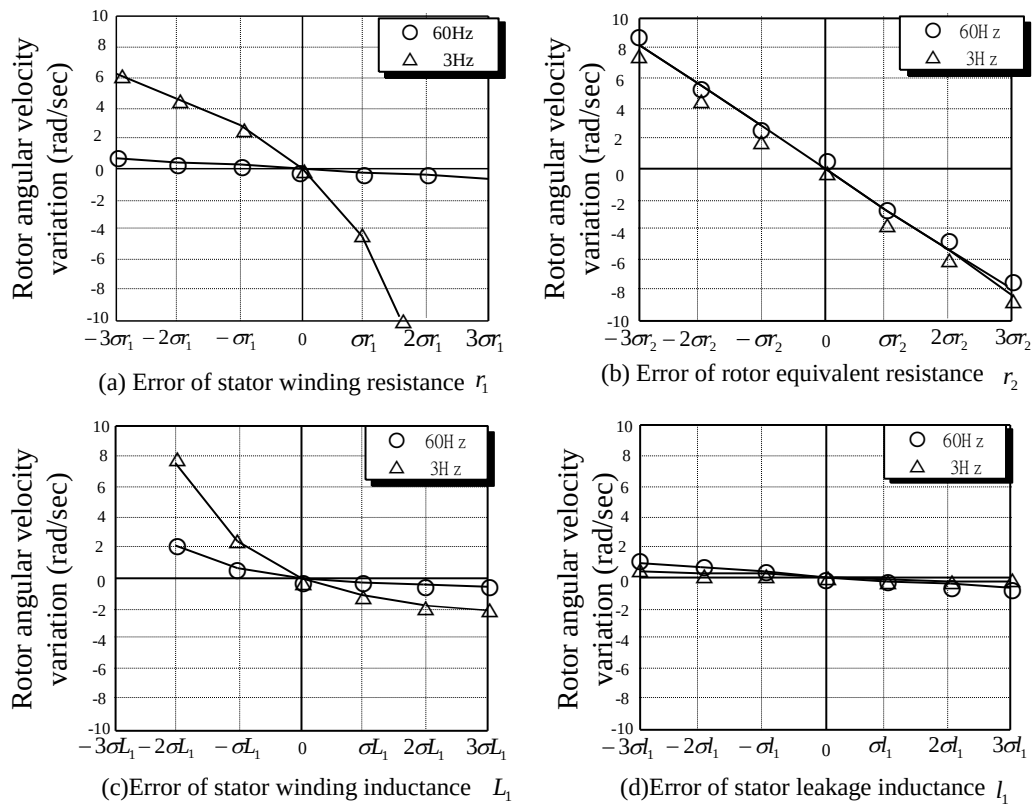

Fig. 4. Relationship between error of induction motor parameters and speed change.

Fig. 4 represents the experimental regulation characteristics of the inductor motor rotor angular speed ω_r under the conditions of not only low frequency at 3Hz but also high frequency at 60Hz in case of giving some errors to the three types of induction motor parameters.

The stator resistance r_1 of the induction motor influences upon the rotor angular speed (ω_r) regulation in the range of low angular frequency ω, its stator inductance influences upon the rotor angular speed regulation over the ranges of high angular frequency ω. It is noted that the rotor resistance r_2 influences upon to the speed regulation for any rotor angular frequency (ω_r) ranges, but the leakage inductance of the stator does not give much influence.

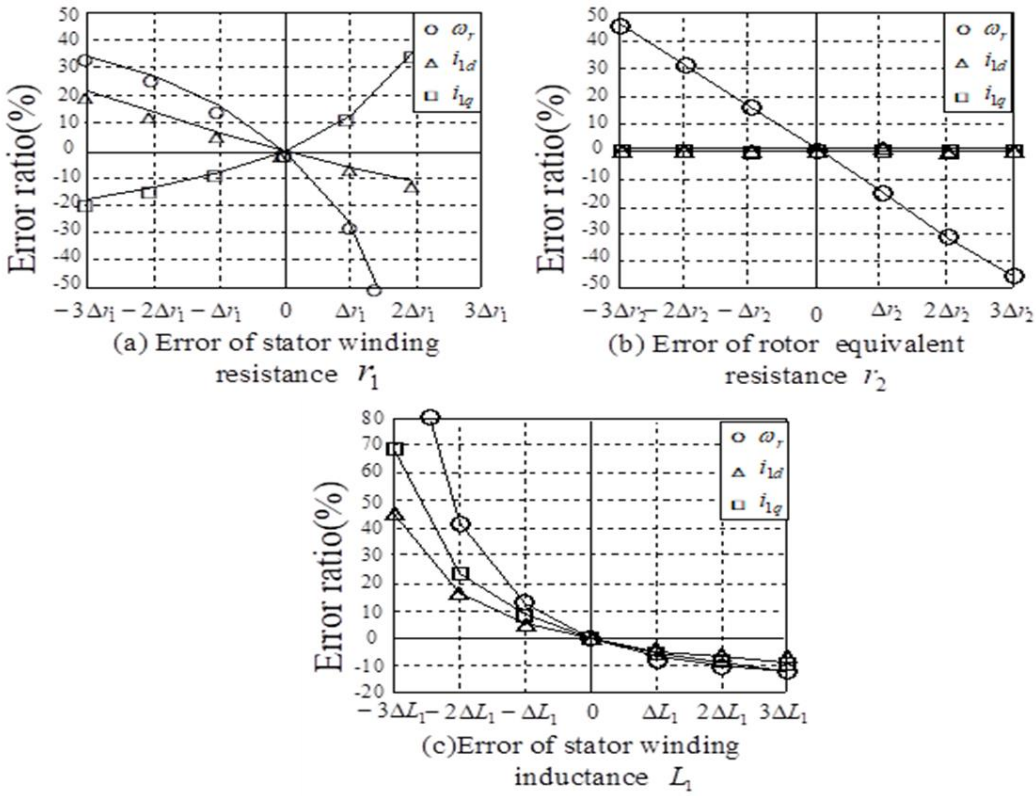

Fig. 5. Relationship between error of induction motor parameters and speed variation

Fig. 5 represents the experimental results of the rotor current regulation to adapt in accordance with some errors to three motor types of machine circuit parameters. Figs. 5(a) and 5(c) show that the variations of the stator resistance and inductance cause the variations of the stator current of which the induction motor. Therefore, it is possible to estimate its stator resistance r_1 and inductance L_1 on the basis of measuring the stator current directly using the sensor consisted by the current transformer and the A/D converter. But Fig. 5(b) shows that the sensor of the rotor angular speed (ω_r) should be necessary to measure the rotor speed ω_r of the induction motor itself because the rotor resistance regulation change the rotor angular speed ω_r but not the stator current. The novel practical automatic estimation or determination scheme of these machine parameters without the rotor angular speed sensing method is discussed and evaluated below.

3.2. 3.2 Estimation of induction motor stator winding resistance

The lumped rotor resistance of the induction motor should be estimated when this induction motor does not rotate to remove the influence upon the stator inductance. Under this condition, the induction motor tested here does not generate the output torque at all, then the torque current component i_{1q} is to be zero. Thus, the following

Equation (7) described as the product of the stator resistance r_1 and the reference value of d-axis exciting current component i_{1d}^* can be exactly derived by substituting $v_{1a} = 0$ to Equation (5).

$$v_{1d} = r_1 i_{1d}^* \tag{7}$$

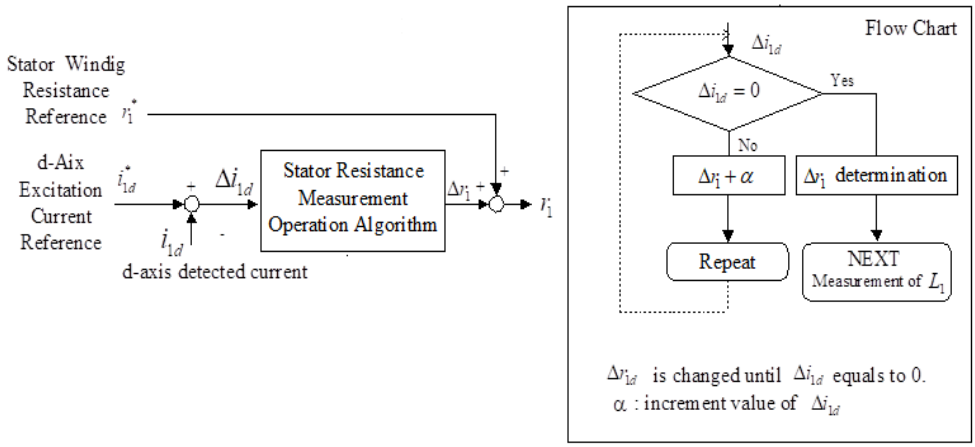

Fig. 6. Schematic block diagram to estimate resistance of induction motor stator.

Fig. 6 demonstrates the practical method to estimate the stator resistance.

The induction-motor stator winding resistance r_1 can be obtained by measuring the current which flows to winding using the current transformer, adding the reference voltage v_{1d}^* determined to the stator coil of the induction motor expressed in equation (7). At the time of opening of measurement, voltage reference value v_{1d}^* determined by the product of the initial current reference value i_{1d}^* and initial stator winding resistance r_1^* which are preset into DSP is added to the primary winding of the induction motor and the actual winding current i_{1d} which flows to induction-motor winding is measured.

If the measured current i_{1d} is equal to the current reference preset value i_{1d}^* the stator winding resistance is equal to the reference resistance r_1^*, but when an error between i_{1d} and i_{1d}^* occurs, the measured resistance r_1 has the error. Since this error current value of Δi_{1d} is generated because of the inequality between the measured resistance value r_1 and the actual resistance value of the induction-motor winding. Therefore, resistance r_1^* is finely tuned until Δi_{1d} of current error by the d-axis current error compensator shown in Fig .6 will be equal to 0 to obtain the exact value of the induction-motor winding resistance, and estimation of the stator resistance will finish after determination r_1 as the actual primary winding resistance value when $\Delta i_{1d} = 0$. As a result, the stator lumped resistance r_1 can be determined exactly.

3.3. 3.3 Estimation of stator inductance

After measuring the stator lumped resistance, the stator inductance can be measured through driving the induction motor for a constant rotor angular speed under no-load condition. In this case, the deviation of angular velocity of the induction motor and the torque current component i_{1q} are both to be zero. Substituting the q-axis current component $i_{1q} = 0$, the equation (5) can be rearranged to the following equations.

$$v_{1d} = r_1 \cdot i_{1d*} v_{1q} = \omega \cdot \varphi \tag{8}$$

where ω is the angular velocity value calculated in vector controlled sesorless inverter system and ϕ is the reference value of flux calculated in vector controlled sesorless inverter system.

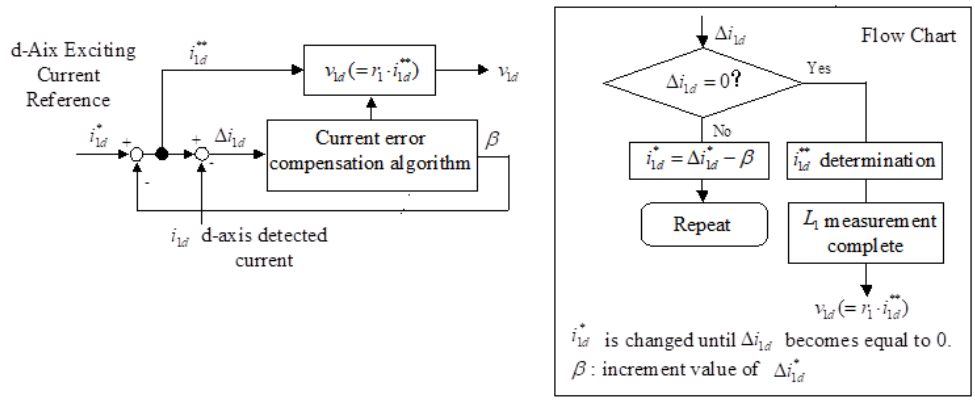

Fig. 7 Schematic block diagram of inductance detector of induction motor stator. $i_{1d}^{*}$is the reference value of exciting current component. i_{1d}^{**} is the preset value of reference exciting current component.

The reference flux ϕ determined by the rated voltage of the induction motor tested here is estimated as the product of the stator inductance L_1 and the exciting or magnetizing current component i_{1q}. That is, we can get,

$$\varphi = L_1 \cdot i_{1d}^{*} \tag{9}$$

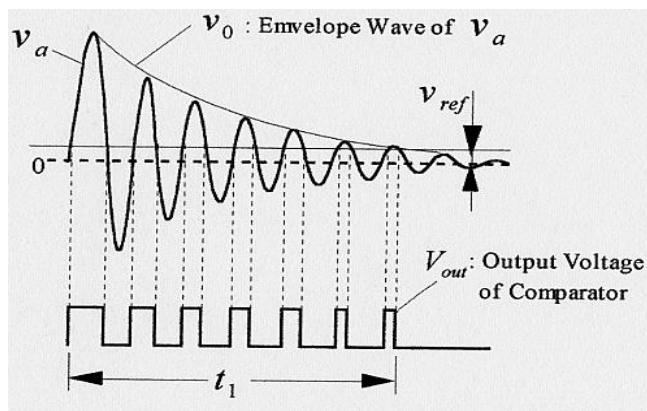

Fig. 8. Relation between residual voltage and output voltage of the comparator output for detection of the induction motor rotor resistance. v_a: Residual voltage waveform between one pair of 3-phase. v_0: Envelope waveform of residual voltage waveform v_a. v_{ref}: Reference voltage value for comparing residual voltage v_a. v_{out}: Output voltage of comparator shown in Fig. 9. t_1: Attenuation period of residual voltage v_a to calculate rotor resistance by substituting to the Equation 16.

In accordance with the equation (9), the mismatched error of L_1 (defined as ΔL_1) of induction motor stator inductance is to be detected as a variation of the exciting current component i_{1d}^{*}. The stator inductance L_1 of the induction motor is measured in terms of the following procedure. The inverter based on the vector controlled scheme has an initial inductance value L_1 of the induction motor preset into the DSP in the control circuit board, if the actual stator inductance L_1 is specified as ΔL_1 larger than the initial preset value of the inverter, exciting current component i_{1d} of the induction motor is smaller as Δi_{1d} which is defined as the equation (10) which is obtained trough substituting $L_1 = L_1 + \Delta L$ into the equation(9) and solving about i_{1d}.

$$\Delta i_{1d} = \frac{\varphi}{(1/(L_1+\Delta L_1)-1/L_1)} \tag{10}$$

Since the stator resistance r_1 of the induction motor has been measured and specified, the difference between the reference value and the detected value of exciting current component Δi_{1d} depends on the mismatched error of the stator inductance of the induction motor used in the electrical system. Therefore, by adjusting the

reference value i_{1d}^{*} of the exciting current component as to be the same as the detected exciting current component i_{1d}, the stator inductance of the induction motor can be exactly set to the actual value L_1. The stator inductance estimation processing scheme is demonstrated in Fig. 7. The current compensator in the control implementation shown Fig.7 adjusts the reference value exciting current component i_{1d}^{*} in order to make the adjusted reference exciting current i_{1d}^{*} equal to the measured stator current i_{1d}.

3.4. Estimation of induction rotor resistance

When the terminals of the induction motor driven by the three-phase sinewave PWM inverter are opened. Absolutely, sinewave voltage v_a across the terminal of the induction motor will decreases gradually. This voltage v_a of which is measured between two wires of three phase voltage is defined as the residual voltage and represented by the following equation which is obtained from the envelope curve of the measured voltage waveform shown in Fig.8.

$$v_a = -\sqrt{2}\omega_r M I_{20} e^{-t/T_0} \cdot sin(\omega_r t + \theta_0) \tag{11}$$

where M is the mutual inductance, ω_r is the rotor angular velocity, I_{20} is the rotor current flowing before opening the power terminal of the induction motor, θ_0 is the initial phase angle expressed generally by sinewave equation, and T_0 is the time constant.

The damping phenomena and performance of a residual phase voltage v_a is determined by the damping time constant T_0 defined as Equation (12). The inductor motor rotor angular speed ω_r, and the induction electrical angular frequency of the residual voltage v_a is equal to the induction motor rotor angular speed ω_r. The damping time constant T_0 is represented as follows by the rotor resistance r_2 and the rotor inductance L_2.

$$T_0 = L_2/r_2 \tag{12}$$

Therefore, the rotor lumped resistance r_2 of the induction motor under the test condition can be calculated from the damping time constant T_0 of the residual voltage v_a detected at the ports of terminal of the induction motor by the circuit of Fig. 9.

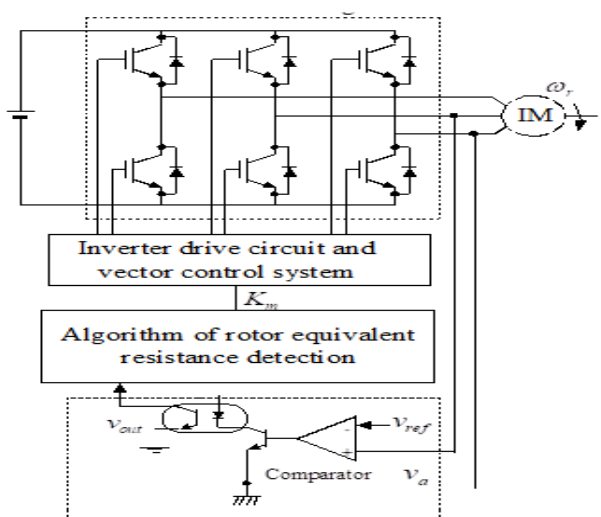

Fig. 9, Schematic diagram of detecting residual voltage for estimation of induction motor rotor resistance. v_a: Residual voltage waveform between one pair of 3-phase.v_{ref}: Reference voltage value for comparing residual voltage v_a to obtain the square wave of the residual voltage waveform. v_{out}: Output voltage of comparator shown in Fig. 9.

Fig. 9 illustrates the easy system which can measure the residual voltage dumping time of the of the induction motor by the DSP without using the A/D conversion.

DSP can recognize the damping time of the residual voltage by the zero-crossing voltage of the residual voltage v_a which generated using 0 crossing comparator comparing with the residual voltage v_a and 0V.

However, in case of zero crossing comparator, the attenuation time of continues very long until the zero-crossing voltage v_{out} fades out completely. Then using the reference voltage, which is little higher than zero volts, the rectangle wave voltage v_{out} of the comparator output will no longer be output when the residual voltage becomes below v_{ref}. Thus, obtained time t_1 shown in Fig. 8 which is the fade-out time of the comparator output voltage v_{out} can be considered the damping time of the residual voltage. Fig. 8 illustrated the relationship between the residual voltage v_a and the output voltage v_{out} of its detecting circuit of Fig. 9. The schematic block diagram of the signal processing circuit to detect the residual voltage v_a was indicated also in Fig. 9. The detecting circuit of the residual voltage composed of a comparator and a photo-coupler is very simple and effective. In Fig.8, when the residual voltage v_a is higher than the comparison reference voltage v_{ref}, the measuring circuit illustrated in the range of the dotted line of Fig.9 generates the square waveform v_{out} output by the comparator shown Fig. 9. By measuring the frequency of comparator output voltage v_{out}, the electrical frequency of the residual voltage v_a can be detected equivalently. As shown in Fig. 9, a novel machine parameter estimation implementation is described in the following. Under the no-load condition, the decreasing of the motor rotor angular speed is too small and can be neglected after opening the induction motor power terminals. Considering the amplitude of the residual voltage v_a, Equation (13) can be obtained as follows.

$$v_{a.} \cong v_0 \cdot e^{-t/T_0} \tag{13}$$

where v_0 is the amplitude of the terminal voltage observed after opening the electrical terminals in the induction motor. Considering the equation (11), v_0 can be calculated as Equation (14)

$$v_0 = \left|-\sqrt{2}\omega_r \cdot M \cdot I_{20}\right| \tag{14}$$

Substituting the observed decreasing time of the residual voltage t_1 to the Equation (13), rearranged equation (15) is obtained from Equations (13) and (14).

$$v_{ref.} \cong v_0 \cdot e^{-t_1/T_0} = \left|-\sqrt{2}\omega_r M I_{20}\right| \cdot e^{-t_1/T_0} \tag{15}$$

For the reasonable conditions of $T_0 = L_2/r_2$, $L_1 \cong L_2$ and Equations (11) - (15) which determine the residual voltage v_a, the rotor resistance r_2 can be given by Equation (16).

$$r_2 = \frac{\varphi_{2d}}{i_{1d} \cdot t_1} ln\left(\frac{v_0}{v_{ref}}\right) \tag{16}$$

where t_1 is a measured period during the residual voltage v_a is larger than v_{ref} in Fig. 8.

By (4), the constant coefficient K_m of the slip angular frequency is required to calculate the slip angular frequency ω_s. The slip angular frequency constant K_m (see Fig.9, 10) is calculated by substitution the r_2 expressed in the Equation (16) to the equation (6) as Equation (17).

$$K_m = \frac{r_2}{\varphi_{2d}} = \frac{1}{i_{1d} \cdot t_1} \ln\left(\frac{v_0}{v_{\text{ref}}}\right) \tag{17}$$

where t_1 is a period when v_a is larger than the reference voltage v_{ref}

Finally, the attenuation time t_1 of the residual voltage is obtained from the square voltage waveform v_{out} of the rotor resistance detective circuit expressed in Fig.8. The slip angular constant K_m defined in the Equation (4) can be calculated by using Equation (17). Because v_0, v_{ref} and t_1 are already known in the Equation (16), the slip angular frequency constant K_m can be obtained easily from the Equation (17). The block diagram for estimating rotor resistance is displayed in Fig.10.

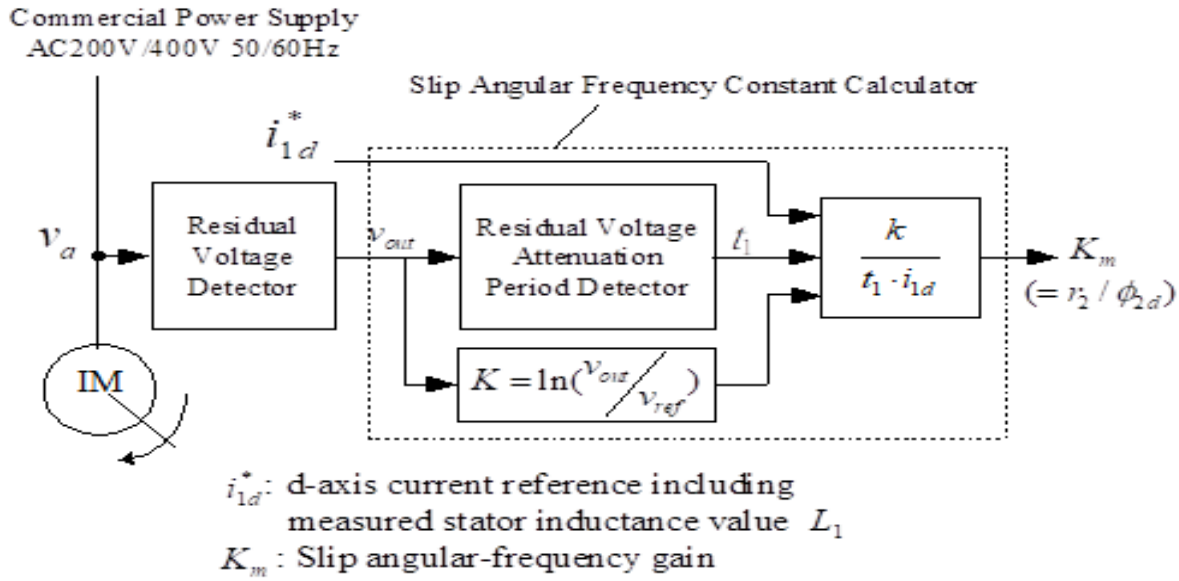

Fig. 10. Block diagram of resistance detector of induction motor rotor

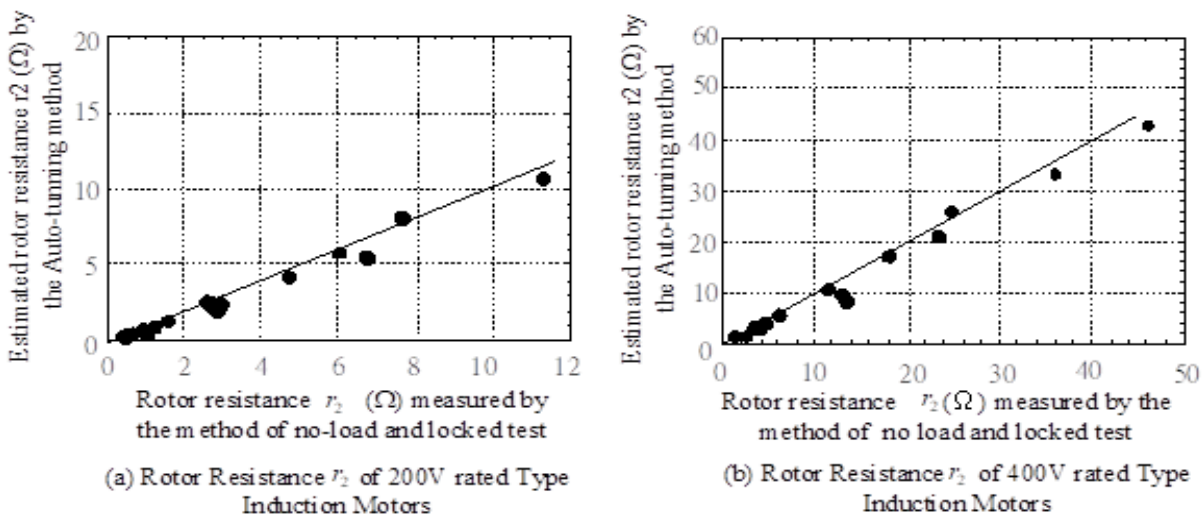

Fig. 11. Rotor resistance values estimated by digital signal processor incorporated into inverter.

Fig. 11 shows the experimental results of some types of induction motors depicted by the estimation system displayed in Fig.10. The induction motors constants are designed for the follow items; Rated voltages are considered for two cases of 200 V and 400 V. The horse powers are regulated from ¼ hp to 5hp. Constructions of the induction motor are considered for three cases of 2, 4 and 6 poles. The difference between the estimated rotor resistance value and one measured by the method obtained by using both no-load test and adjustable speed induction motor drive system with its machine parameter measuring scheme is implemented in Fig.12.

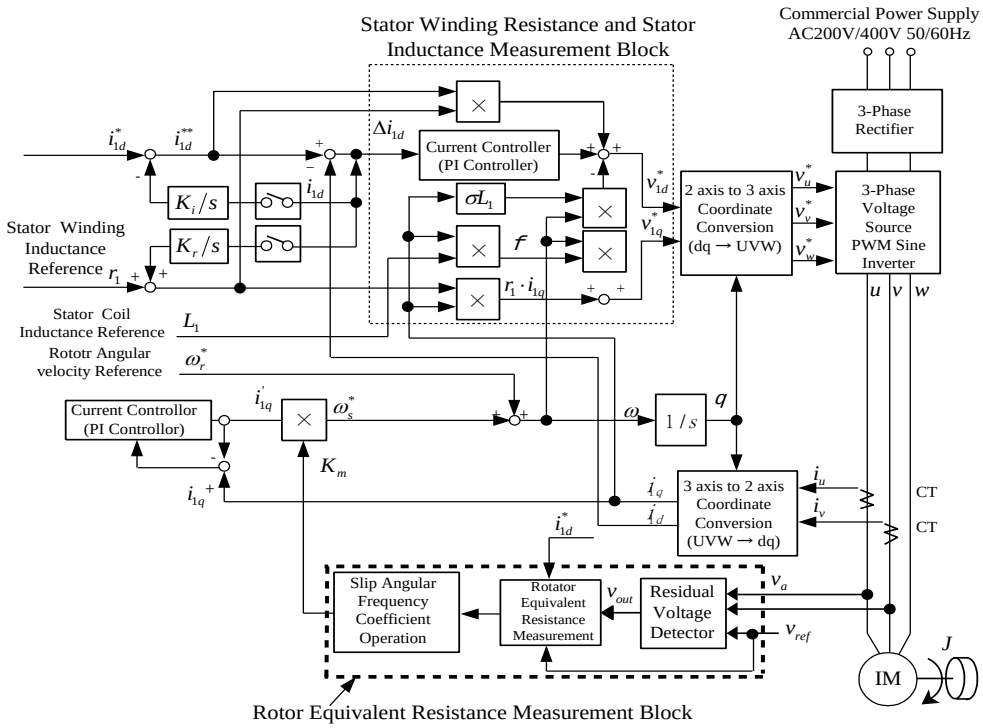

Fig. 12. Block diagram of control system with a novel auto-turning machine parameter estimation scheme.

4. SYSTEM IMPLEMENTATION

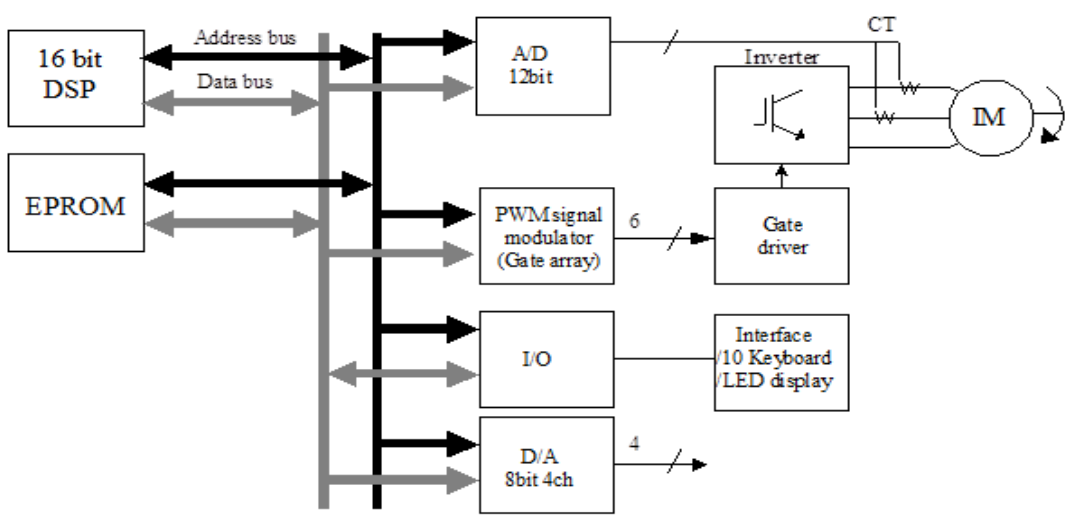

Fig. 13. Feasible DSP circuit implementation of vector inverter.

The feasible system implementation of the three-phase PWM inverter-fed induction motor drive is concretely depicted in Fig 13. The slip frequency-based sensorless vector control software processing stage and the calculation processing stage of the delay torque current component can be achieved in terms of DSP implementation with its peripheral circuits including operational amplifier, A/D converters, D/A converters and so on as depicted in Fig.13. In this case, the control procedures for the d-q coordinate transformation processing and the reference voltage can be achieved within 100 μsec. The induction machine parameter estimations and

the calculation processing of the delay torque current component in dynamic state can be performed during the sampling time $T_s = 1\ msec$. Also, in this machine parameter estimation system, the current detection interface board designed by the authors uses the isolated current transformer CT with hall-effect sensing device and 12-bit A/D converter.

5. EXPERIMENTAL RESULTS AND PRACTICAL EVALUATIONS

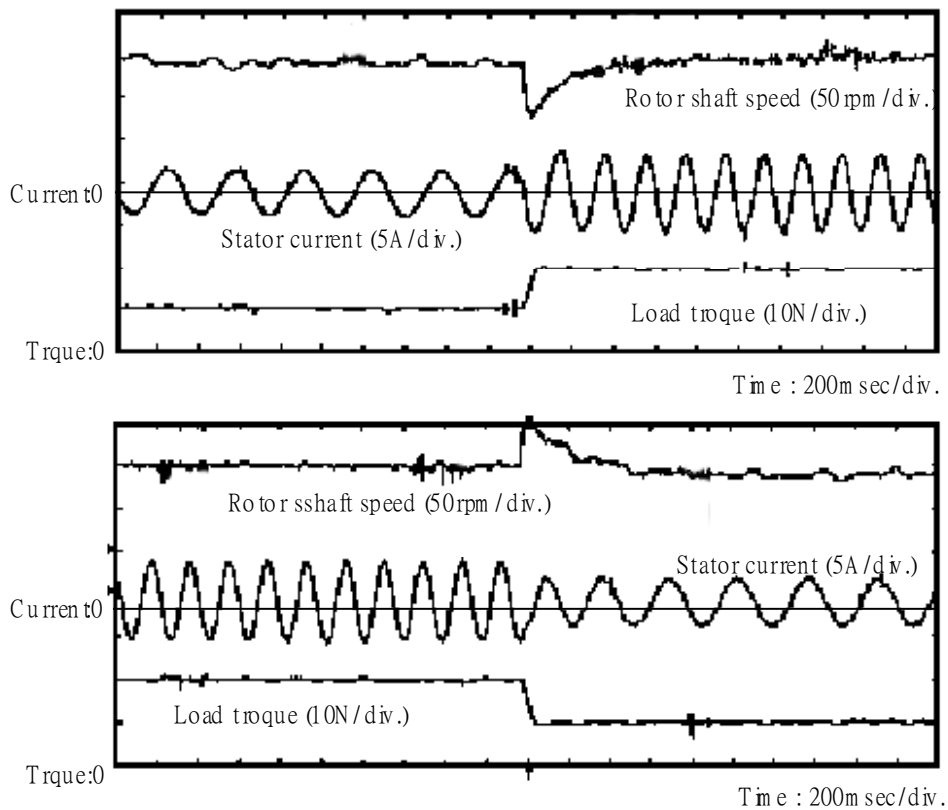

Fig. 14. Step speed response in case of load torque change.

Fig. 14 illustrates the dynamic speed transient response performances when step-rise load torque disturbance is applied for this induction motor drive system from no-load to full load torque.

It is proven from a practical point of view in practice that the stator current of the induction motor adjustable speed system driven by the three-phase PWM inverter using sensorless slip frequency-based vector control scheme system becomes stable without an excessive current despite largely changed load torque disturbances. In addition to this, in experiment, the speed regulation factor in steady state is less than about 2.8% of the rated speed over wide speed ranges settings as well as large load torque disturbances. Furthermore, it is noted that the transient recovering time or settling time is to be about 300 msec. Table 1 indicates the induction motor machine constants measured by means of no-load test and lock test.

Fig. 15 illustrates the steady state torque vs. speed characteristics of this the induction motor speed control scheme. It is noted that the steady state accuracy of the speed regulation for two types of induction motors is less than about 2% within a wide range of speed settings and under load torque variation conditions.

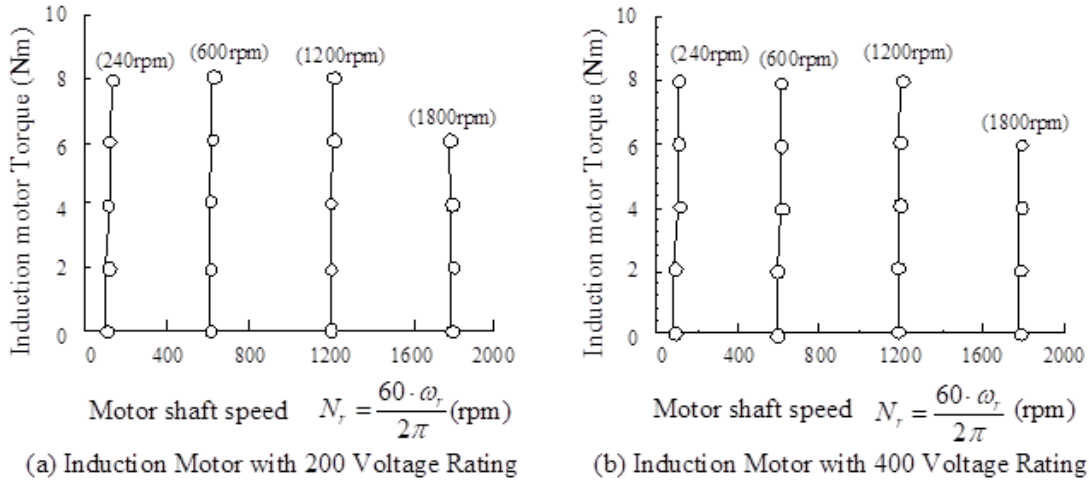

Fig. 15. Characteristics between motor speed and torque estimated by novel machine parameter auto-tuning method.

TABLE1 MACHINE PARAMETERS.

Motor	r1(Ω)	r2(Ω)	L1 (H)
Type A	2.50	2.47	0.15
Type B	1.54	1.97	0.11

6. CONCLUSIONS

In this paper, demonstrated and characterized are, a high performance and accurate adjustable-speed induction motor drive system incorporating sensorless slip frequency type vector control based three-phase voltage source type sinewave PWM inverter using IGBTs power modules. The high frequency carrier PWM sinewave three-phase inverter operating under current controlled voltage source has a novel automatic auto-tuning induction machine circuit parameter estimation scheme in addition to an effective PI controller to delay the transient torque current component to reduce the excessive induction motors stator current in the dynamic load torque disturbances. The inherent automatic auto-tuning principle of the stator and rotor circuit parameters of some types of general-purpose induction motors has been presented including actual measuring processing from theoretical and practical considerations. Finally, the steady state variable speed regulation characteristics and dynamic speed response performances of cost effective sensorless vector control inverter-fed induction motor variable speed drive system have been built and tested experimentally.

Acknowledgement

The authors extend their appreciation to the Sohag University for funding this work under project number No.: 201920, funded by Sohag University (Call 2019).

REFERENCES

[1] Tung-Hai Chin, "Sensorless Vector Control for Induction motor," *IEE Japan Trans. on IAS*. Vol.112 pp.167-175, Mar. 1992.

[2] K. Ohnishi, "Decoupling Control of Secondary Flux And Secondary Current In Induction Motor Drive With Controlled Voltage Source and Its Comparison With Volt/Herz Control"; *Rec. of IEEE/IAS Annual Meeting Conf. Rec*. pp. 678-685, Oct., 1982.

[3] Tung-Hai Chin, "Hyperstability of the Full Order Adaptive Observer fir Vector Controlled-Induction Motor Drive without Speed-Sensor," IEE Trans. on IAS. Vol.112. No.//pp.1047-1055, Nov. 1992

[4] T. Okuyama, “Vector Control Scheme of Induction Motor without Speed and Voltage Sensors,” *IEE Japan Trans. on IAS.* Vol.107. No.2 pp.191-198, Feb. 1987.

[5] N. Yamamura, “PG-less Vector Control with Estimating Functions of Motor Parameter,” *IEE Japan Trans. on IAS.* Vol.107. No5. pp.373-378, May, 1991.

[6] T. Okuyama, "Simplified Vector Control System without Speed and Voltage Sensors - Effect of Setting Errors in Control Parameters and their Compensation "; IEE Japan Trans. on IAS. Vol.110. pp.477-486, May, 1990

[7] Y. Okamura, "Speed Sensorless Control Scheme With Motor Parameter Identification Function for Vector Controlled Induction Motor Drives "; IEE Japan Technical Report of Rotation Machinery, RM-94-62, pp.21-30, Jun. 1994.

[8] Y. Okamura, “High Performance Adjustable-Speed Induction Motor Drive System using Sensorless Vector Controlled PWM Inverter with Auto-Tuning Machine-Operated Parameter Estimation Schemes,” *Powersystems World - Intelligent Motion System*, pp.204-223, Sept. 1995.

[9] Y. Okamura, **“**High Performance Adjustable-Speed Induction Motor Drive System using Sensorless Vector Control-based PWM Inverter with Auto-Tuning Machine-Operated Parameter Estimation Schemes”; Proc. of IEE-Korea International Conference on Power Electronics pp. 804-809, Oct. 1995.

[10] R. Kassem, K. Sayed, A. Kassem, and R. Mostafa, “Power optimisation scheme of induction motor using FLC for electric vehicle,” *IET Electrical Systems in Transportation*, Vol. 10, No. 3, pp. 301-309, 2020..

[11] Ahmed G. Abo-Khalil, Ali M. Eltamaly, Mamdooh S. Alsaud, Khairy Sayed, Ali S. Alghamdi, “Sensorless control for PMSM using model reference adaptive system," International Transaction Electrical Energy System, Vol. 31, No. 2, 2021.

[12] K. Sayed, A. Kassem, H. Saleeb, A. S. Alghamdi, A. G. Abo-Khalil, “Energy-Saving of Battery Electric Vehicle Powertrain and Efficiency Improvement during Different Standard Driving Cycles,” *Sustainability*. Vol. 12, No. 24, pp. 301-309, 2020.

[13] Ali S. Alghamdi, Khairy Sayed, Ahmed G. Abokhalil, Ahmed Bilal Awan, Mohamed A. Zohdy, “A Soft Switching DC-Link Quasi Resonant Three-Phase Inverter for AC Servo-Motor Drive Applications,” *International Transaction Journal of Engineering, Management, & Applied Sciences & Technologies*, Vol. 12, No. 1, pp. 1-13, 2021.

[14] A. M. Eltamaly, M. Al-Saud, K. Sayed, and A. G. Abo-Khalil, "Sensorless Active and Reactive Control for DFIG Wind Turbines Using Opposition-Based Learning Technique," *Sustainability*, Vol. 12, No. 9, p. 3583, 2020.

[15] R. Kassem, K. Sayed, A. Kassem, R. Mostafa, ""Energy Efficient Control Scheme of Induction Motor Based EV,” 21st International Middle East Power Systems Conference (MEPCON), 2019. https://doi.org/10.1002/2050-7038.12733

[16] Liying Liu, Zhenlin Xu and Qiang Mei, “A sensorless vector control induction motor drive based on ADRC and flux observer,” 2009 Chinese Control and Decision Conference, Guilin, China, 2009, pp. 945-948, doi: 10.1109/CCDC.2009.5191888.

[17] J. Titus, P. Harikrishnan and K. Hatua, "Sensorless Vector Control for a Load Commutated Inverter fed Active-Reactive Induction Motor Drive," 2019 IEEE 13th International Conference on Compatibility, Power Electronics and Power Engineering (CPE-POWERENG), Sonderborg, Denmark, 2019, pp. 1-6, doi: 10.1109/CPE.2019.8862386.

[18] A. Iqbal and M. R. Khan, "Sensorless control of a vector controlled three-phase induction motor drive using artificial neural network," 2010 Joint International Conference on Power Electronics, Drives and Energy Systems & 2010 Power India, New Delhi, India, 2010, pp. 1-5, doi: 10.1109/PEDES.2010.5712474.

[19] J.Mohanalakshmi and H. N. Suresh, “Sensorless speed estimation and vector control of an Induction Motor drive using model reference adaptive control,” 2015 International Conference on Power and Advanced Control Engineering (ICPACE), Bengaluru, India, 2015, pp. 377-382, doi: 10.1109/ICPACE.2015.7274976.

[20] B. Renukrishna and S. S. Beevi, "Sensorless vector control of induction motor drives using rotor flux observer," 2012 IEEE International Conference on Power Electronics, Drives and Energy Systems (PEDES), Bengaluru, India, 2012, pp. 1-5, doi: 10.1109/PEDES.2012.6484463.